THE JOURNAL OF BIOLOGICAL CHEMISTRY VOL. 281, NO. 49, pp. 37675–37685, December 8, 2006

Association of Kv1.5 and Kv1.3 Contributes to the Major Voltage-dependent K^+ Channel in Macrophages*

Received for publication, June 12, 2006, and in revised form, September 28, 2006 Published, JBC Papers in Press, October 11, 2006, DOI 10.1074/jbc.M605617200

Rubén Vicente[‡1,2], **Artur Escalada**[§1,3], **Nuria Villalonga**[‡4], **Laura Texidó**[§], **Meritxell Roura-Ferrer**[‡5], **Mireia Martín-Satué**[§], **Carmen López-Iglesias**[¶], **Concepció Soler**[‖6], **Carles Solsona**[§7], **Michael M. Tamkun**[**1,8], **and Antonio Felipe**[‡1,9]

From the [‡]*Molecular Physiology Laboratory, Departament de Bioquímica i Biologia Molecular,* [‖]*Departament de Fisiologia, and* [¶]*Unitat de Reconeixement Molecular in situ, Serveis Cientificotècnics Universitat de Barcelona, E-08028 Barcelona, Spain,* [§]*Cellular and Molecular Neurobiology Laboratory, Departament de Patologia i Terapèutica Experimental (IDIBELL), Universitat de Barcelona-Campus de Bellvitge, E-08907 Hospitalet de Llobregat, Spain, and* **Department of Biomedical Sciences, Colorado State University, Fort Collins, Colorado 80523*

Voltage-dependent K^+ (Kv) currents in macrophages are mainly mediated by Kv1.3, but biophysical properties indicate that the channel composition could be different from that of T-lymphocytes. K^+ currents in mouse bone marrow-derived and Raw-264.7 macrophages are sensitive to Kv1.3 blockers, but unlike T-cells, macrophages express Kv1.5. Because *Shaker* subunits (Kv1) may form heterotetrameric complexes, we investigated whether Kv1.5 has a function in Kv currents in macrophages. Kv1.3 and Kv1.5 co-localize at the membrane, and half-activation voltages and pharmacology indicate that K^+ currents may be accounted for by various Kv complexes in macrophages. Co-expression of Kv1.3 and Kv1.5 in human embryonic kidney 293 cells showed that the presence of Kv1.5 leads to a positive shift in K^+ current half-activation voltages and that, like Kv1.3, Kv1.3/Kv1.5 heteromers are sensitive to r-margatoxin. In addition, both proteins co-immunoprecipitate and co-localize. Fluorescence resonance energy transfer studies further demonstrated that Kv1.5 and Kv1.3 form heterotetramers. Electrophysiological and pharmacological studies of different ratios of Kv1.3 and Kv1.5 co-expressed in *Xenopus* oocytes suggest that various hybrids might be responsible for K^+ currents in macrophages. Tumor necrosis factor-α-induced activation of macrophages increased Kv1.3 with no changes in Kv.1.5, which is consistent with a hyperpolarized shift in half-activation voltage and a lower IC_{50} for margatoxin. Taken together, our results demonstrate that Kv1.5 co-associates with Kv1.3, generating functional heterotetramers in macrophages. Changes in the oligomeric composition of functional Kv channels would give rise to different biophysical and pharmacological properties, which could determine specific cellular responses.

Voltage-dependent potassium channels (Kv)[10] have a crucial function in excitable cells of determining resting membrane potential and controlling action potentials (1). In addition, they are involved in the activation and proliferation of leukocytes (2). Functional Kv complexes are formed by four transmembrane α subunits and up to four cytoplasmic β subunits (3). The mammalian *Shaker* family (Kv1) contains at least eight different genes (Kv1.1–Kv1.8), coding for α subunits, which form functional homo- and heterotetrameric complexes. Thus, Kv1 proteins can assemble promiscuously, yielding a wide variety of biophysically and pharmacologically distinct channels (4, 5). However, although a number of studies have demonstrated that specific Kv heteromeric complexes predominate in nerve and muscle, many other possible combinations go undetected (6, 7). Therefore, this mechanism of channel assembly may underlie some of the functional diversity of potassium currents found in the brain and the cardiovascular system.

Bone marrow-derived macrophages (BMDM) are fully differentiated cells. In response to different growth factors and cytokines, macrophages can proliferate, become activated, or differentiate. These cells have a key function at inflammatory loci, where they arrive 24–48 h after lesion and remain until inflammation disappears. However, the persistence of macrophages at inflammatory loci is associated with the pathogenesis of a wide range of inflammatory diseases. Kv are tightly regulated during proliferation and activation in macrophages, and their functional activity is important for cellular responses (8). Proliferation and activation trigger an induction of the outward K^+ current that is under transcriptional and translational control (8). Several lines of evidence indicate that post-translational events are involved in Kv regulation. In this context,

* The costs of publication of this article were defrayed in part by the payment of page charges. This article must therefore be hereby marked "*advertisement*" in accordance with 18 U.S.C. Section 1734 solely to indicate this fact.
[1] These authors contributed equally to this work.
[2] Holds a fellowship from the Universitat de Barcelona.
[3] Supported by a fellowship from the Fundació Marató TV3.
[4] Holds a fellowship from the Ministerio de Educación y Ciencia.
[5] Hold a fellowship from the Generalitat de Catalunya.
[6] Supported by the Fondo de Investigaciones Sanitarias (PI021192) and the Ramón y Cajal program of the Ministerio de Educación y Ciencia.
[7] Supported by the Fundació August Pi i Sunyer, Generalitat de Catalunya, and the Ministerio de Educación y Ciencia (BFI2001-3331, SAF2005-00736).
[8] Supported by National Institutes of Health Grants HL49330 and NS41542.
[9] Supported by the Ministerio de Educación y Ciencia, Spain (BFI2002-00764, BFU2005-00695). To whom correspondence should be addressed: Molecular Physiology Laboratory, Departament de Bioquímica i Biologia Molecular, Universitat de Barcelona, Avda. Diagonal 645, E-08028 Barcelona, Spain. Tel.: 34-93-4034616; Fax: 34-93-4021559; E-mail: afelipe@ub.edu.

[10] The abbreviations used are: Kv, voltage-dependent potassium channels; BMDM, bone marrow-derived macrophages; MgTx, rMargatoxin; HEK, human embryonic kidney 293; RT, reverse transcription; PBS, phosphate-buffered saline; FRET, fluorescence resonance energy transfer; TNF, tumor necrosis factor.

assigning specific K^+ channel clones to native currents is difficult, since this complexity is further enhanced by heteromultimeric assembly of different Kv subunits. Lymphocytes express several voltage-dependent K^+ currents (*n, n′*, and *l*-type channels). Although Kv1.3, the major Kv channel in leukocytes, is associated with the *n*-type channel and Kv3.1 accounts for the *l*-type, the proteins responsible for the *n′*-type are unknown (2). Electrophysiological properties such as activation and inactivation of Kv1.3 expressed in T-cells and heterologous expression systems (Refs. 9 and 10 and references herein) are significantly different from those described in macrophages (8, 10, 11). In addition, unlike T-lymphocytes, brain and bone marrow macrophages also express Kv1.5 (8, 10, 11–15). Kv1.3 and Kv1.5 differ in their biophysical and pharmacological properties and show distinct regulation in a number of cell types (8, 16–18). Thus, different K^+ channel subunit composition could lead to specific alteration of cellular excitability, thus determining specific cell responses.

The aim of the present study was to explore whether Kv1.5 has a function in the major voltage-dependent K^+ current in macrophages. Our results suggest that Kv1.5 co-associates with Kv1.3, generating functional Kv1.3/Kv1.5 heterotetrameric channels. Upon different physiological stimuli, changes in the oligomeric composition of functional Kv could have a crucial effect on intracellular signals, determining the specific macrophage response.

EXPERIMENTAL PROCEDURES

Animals and Cell Culture—BMDM and Raw 264.7 macrophages, human embryonic kidney 293 (HEK-293) cells, EL-4 T cell line, and *Xenopus laevis* oocytes were used. BMDM from 6–10-week-old BALB/c mice (Charles River Laboratories) were isolated and cultured as described elsewhere (8). Briefly, animals were killed by cervical dislocation, and both femurs were dissected with adherent tissue removed. The ends of bones were cut off, and the marrow tissue was flushed by irrigation with medium. The marrow plugs were passed through a 25-gauge needle for dispersion. The cells were cultured in plastic dishes (150 mm) in Dulbecco's modified Eagle's medium containing 20% fetal bovine serum and 30% L-cell-conditioned media as a source of macrophage-colony stimulating factor. Macrophages were obtained as a homogeneous population of adherent cells after 7 days of culture and maintained at 37 °C in a humidified 5% CO_2 atmosphere. Raw 264.7 macrophages and EL-4 and HEK-293 cells were cultured in Dulbecco's modified Eagle's medium culture media containing 10% fetal bovine serum supplemented with 10 units/ml penicillin and streptomycin and 2 mM L-glutamine. Cells were grown in 100-mm tissue culture dishes for sample collection and on non-coated glass coverslips for electrophysiology and confocal imaging. In some experiments Raw 264.7 cells were incubated with 100 ng/ml recombinant TNF-α (PrepoTech E) for 24 h. All animal handling was approved by the ethics committee of the University of Barcelona and was in accordance with European Union regulations.

RNA Isolation and RT-PCR Analysis—Total RNA from tissues (brain, liver) and cell lines was isolated using the Tripure isolation reagent (Roche Diagnostics). To avoid DNA contamination, the obtained RNA was treated with DNase I, and additional PCR controls were performed in the absence of reverse transcriptase. Ready-to-Go RT-PCR beads (Amersham Biosciences) were used in a one-step RT-PCR reaction. Total RNA and Kv1.3 and Kv1.5 primers were added to the beads as described (8, 11, 19). Forward and reverse oligonucleotide sequences and accession numbers were as follows: Kv1.3 (accession number M30441; forward, 5′-CTCATCTCCATTGTCATCTTCTGA-3′, base pairs 741–765; reverse, 5′-TTGAAGTTGGAAACAATCAC-3′, base pairs 1459–1440); Kv1.5 (accession number AF302768, forward, 5′-GGATCACTCCATCACCAG-3′, base pairs 3003–3020; reverse, 5′-GGCTTCCTCCTCCTTCCTTG-3′, base pairs 3337–3320). The RT reaction was initiated by incubating the mixture at 42 °C for 30 min. Once the first-strand cDNA was synthesized, the conditions were set for further PCR: 92 °C for 30 s, 58 °C for 1 min, and 72 °C for 1 min. These settings were applied for 30 cycles.

Protein Extracts, Immunoprecipitation, and Western Blot—Cells were washed twice in cold phosphate-buffered saline (PBS) and lysed on ice with lysis solution (1% Nonidet P-40, 10% glycerol, 50 mmol/liter HEPES, pH 7.5, 150 mmol/liter NaCl) supplemented with 1 μg/ml aprotinin, 1 μg/ml leupeptin, 86 μg/ml iodoacetamide, and 1 mM phenylmethylsulfonyl fluoride as protease inhibitors. To obtain enriched membrane preparations, homogenates were centrifuged at 3,000 $\times$ *g* for 10 min, and the supernatant was further centrifuged at ~150,000 $\times$ *g* for 90 min. The pellet was resuspended in 30 mM HEPES, pH 7.4, and protein content was determined by Bio-Rad protein assay. Samples were separated into aliquots and stored at −80 °C.

Crude membrane protein samples (50 μg) were boiled in Laemmli SDS loading buffer and separated on 10% SDS-PAGE. They were transferred to nitrocellulose membranes (Immobilon-P, Millipore) and blocked in 5% dry milk-supplemented 0.2% Tween 20 PBS before immunoreaction. Filters were immunoblotted with antibodies against Kv1.3 (1/200, Alomone) and Kv1.5 (1/500, Alomone). As a loading and transfer control, a monoclonal anti-β-actin antibody (1/5000, Sigma) was used. The specificity of Kv1.3 and Kv1.5 commercial antibodies was tested with control antigen peptides provided by the manufacturer.

For immunoprecipitation studies, membrane pellets were resuspended in 1% Triton, 10% glycerol, 50 mM HEPES, pH 7.2, 150 mM NaCl incubated in the presence of protein A-Sepharose, and pelleted. Supernatants incubated overnight with anti-Kv1.3 antibody (Alomone) were further incubated with protein A-Sepharose, washed with 0.1% Triton/PBS, and centrifuged. Pellets were re-suspended in Laemmli SDS-loading buffer, boiled at 95 °C, and separated on 8% SDS-PAGE. To detect immunoprecipitated Kv1.5, an anti-Kv1.5 antibody (1/250) produced and characterized in the Tamkun laboratory was used. Densitometric analysis of the filters was performed by Phoretix software (Nonlinear Dynamics). Results are the mean ± S.E. of each experimental group.

DNA Constructs, Cell Transfection, and Microinjection—Rat Kv1.3 cDNA, kindly donated by T. C. Holmes (New York University), was amplified by PCR and ligated into pEYFP-C1 (Clontech) by using BglII and HinDIII restriction sites. Human

Kv1.5 cDNA was amplified by PCR and ligated into pECFP-C1 (Clontech) by using BglII and EcoRI. Both constructs were verified by sequencing.

Raw 264.7 and HEK cells were grown on glass coverslips in 35-mm dishes, and transient transfection was performed using Lipofectamine 2000 (Invitrogen) to near 80% confluency. Twenty-four hours after transfection, cells were washed with PBS, fixed, and mounted with Aqua Poly/Mount from Polysciences, Inc.

X. laevis oocytes were prepared and injected by standard methods. Mature female frogs were purchased from the Centre d'Elevage de Xenopes (Montpellier, France). Animals were anesthetized in cold distilled water containing 1.7 g/liter tricaine(ethyl 3-aminobenzoate methanesulfonic acid; Sigma). Ovarian sacs were extracted by sterile surgical procedures and placed in sterile Barth's solution (88 mM NaCl, 1 mM KCl, 0.33 mM $Ca(NO_3)_2$, 0.41 mM $CaCl_2$, 0.82 mM $MgSO_4$, 2.40 mM $NaHCO_3$, and 20 mM HEPES at pH 7.5 supplemented with penicillin 100 IU/ml and streptomycin 0.1 mg/ml). Oocytes at stages V and VI were dissected out and kept at 15–16 °C in sterile Barth's solution.

Full-length Kv1.3 and Kv1.5 were subcloned into pcDNA3. cRNAs were generated with T7 RNA polymerase by using the mMESSAGE mMACHINE kit according to manufacturer's instructions (Ambion). Oocytes were injected with 10 ng of Kv1.3 or Kv1.5 of *in vitro* transcribed cRNAs to form homotetramers. Heterotetramers were expressed in oocytes injected with 10 ng of total cRNA of Kv1.3 and Kv1.5 in the proportions of 1:1, 3:1, and 1:3 using a Variable Nanoject (Drummond Scientific Co). Twenty-four hours after injection, the follicular cell layer was partially removed by incubation for 30 min with 0.25 mg/ml type-1A collagenase (Sigma). Oocytes were maintained at 15–16 °C in sterile Barth's solution, and recordings were made 3 days later.

Confocal Imaging and Fluorescence Resonance Energy Transfer (FRET) Experiment—Transient transfected cells were fixed with 4% paraformaldehyde, PBS for 10 min. Acceptor photobleaching method was used to measure the FRET. Fluorescent proteins from fixed cells were excited with the 458-nm or the 514-nm lines by low excitation intensities and 475–495-nm bandpass and >530-nm longpass emission filters, respectively. Subsequently, YFP protein was bleached by using maximum laser power, obtaining around 80% of acceptor intensity bleaching. After photobleaching images of the donor and acceptor were taken, FRET efficiency was calculated as $((F_{CFPafter} - F_{CFPbefore})/F_{CFPafter}) \times 100$, where $F_{CFPafter}$ is the intensity of fluorescence of donor after bleaching, and $F_{CFPbefore}$ is before bleaching. Loss of fluorescence intensity was corrected by measuring CFP intensity in the non-bleached part of the cell. The FRET values are expressed as the means ± S.E. of $n > 10$ cells for each population.

Electron Microscopy—Cells were fixed in 4% paraformaldehyde, 0.2% glutaraldehyde in PBS for 30 min at room temperature and then replaced with 2% paraformaldehyde, 0.1% glutaraldehyde in PBS overnight at 4 °C. Fixation was removed by washing with 0.02 M glycine in PBS. Cells were scraped and collected in Eppendorf tubes with 12% gelatin. After solidifying on ice, gelatin blocks were infiltrated in 2.3 M sucrose in PBS overnight at 4 °C. Blocks were frozen in liquid nitrogen. Ultrathin cryosections were obtained using Leica ULTRACUT EM FCS at −118 °C and subjected to immunogold labeling. Cryosections were incubated at room temperature on drops of 2% gelatin in phosphate buffer for 20 min at 37 °C followed by 50 mM glycine in PBS for 15 min and 5% normal goat serum in PBS for 10 min. Then they were incubated with anti-Kv1.5 or and anti-Kv1.3 polyclonal antibodies in 5% normal goat serum in PBS for 30 min. After 3 washes with drops of 5% normal goat serum in PBS for 20 min, sections were incubated for 60 min using IgG anti-rabbit coupled to 10-nm or to 15-nm diameter colloidal gold particles (Aurion) using a 1:60 dilution in 5% normal goat serum in PBS. This was followed by 3 washes with drops of PBS for 10 min and 2 washes with distilled water. As a control for nonspecific binding of the colloidal gold-conjugated antibody, the primary polyclonal antibody was omitted. Finally, the cryosections were contrasted and embedded in a mixture of methylcellulose and uranyl acetate. At the double immunogold, an immunolabeling with one of the primary antibodies was done. In the first immunolabeling procedure we used the secondary antibody conjugated with the small gold (10 nm). Then the inactivation of the anti-IgG binding sites, using 3% paraformaldehyde, 2% glutaraldehyde in PBS for 2 h, was performed (20). After inactivation the immunolabeling with the other primary antibody was done using in this case the secondary antibody conjugated to 15-nm gold particles. Primary antibody dilutions were 1:50 in both cases. Samples were viewed with a Jeol 1010 electron microscope.

Electrophysiological Recordings—Whole-cell currents were measured with the patch clamp technique. An EPC-9 (HEKA) amplifier with the appropriate software was used for data recording and analysis. Currents were filtered at 2.9 kHz. Series resistance compensation was always above 70%. Patch electrodes of 2–4 megaohms were fabricated in a P-97 puller (Sutter Instruments Co.) from borosilicate glass (outer diameter of 1.2 mm and inner diameter of 0.94 mm; Clark Electromedical Instruments Co). Electrodes were filled with the 120 mM KCl, 1 mM $CaCl_2$, 2 mM $MgCl_2$, 10 mM HEPES, 11 mM EGTA, 20 mM D-glucose adjusted to pH 7.3 with KOH. The extracellular solution contained 120 mM NaCl, 5.4 mM KCl, 2 mM $CaCl_2$, 1 mM $MgCl_2$, 10 mM HEPES, 25 mM D-glucose adjusted to pH 7.4 with NaOH. After establishment of a whole-cell configuration, macrophages were clamped to a holding potential of −60 mV, with seal resistances of at least 2.5 gigaohms. All recordings were routinely subtracted for leak currents at −50 mV online. Only cells with a series resistance compensation of 80–90% were selected for analysis. Uncompensated series resistances were 4–8 megaohms, as currents evoked were less than 1nA; voltage errors from uncompensated series resistance were less than 2 mV.

To determine voltage dependence of steady-state activation, currents were elicited by 200-ms voltage pulses (−50 to +50 mV, V_h) from a holding potential V_h of −60 mV with 10-mV increments. To ensure complete recovery from inactivation, cells were repolarized for 45 s at −60 mV. After converting the steady-state peak outward currents (I_k) into conductances, G_k ($G_k = I_k/(V_h - E_k)$; E_k, Nernst potential of K^+ −79 mV), conductances at various membrane potentials were normalized to

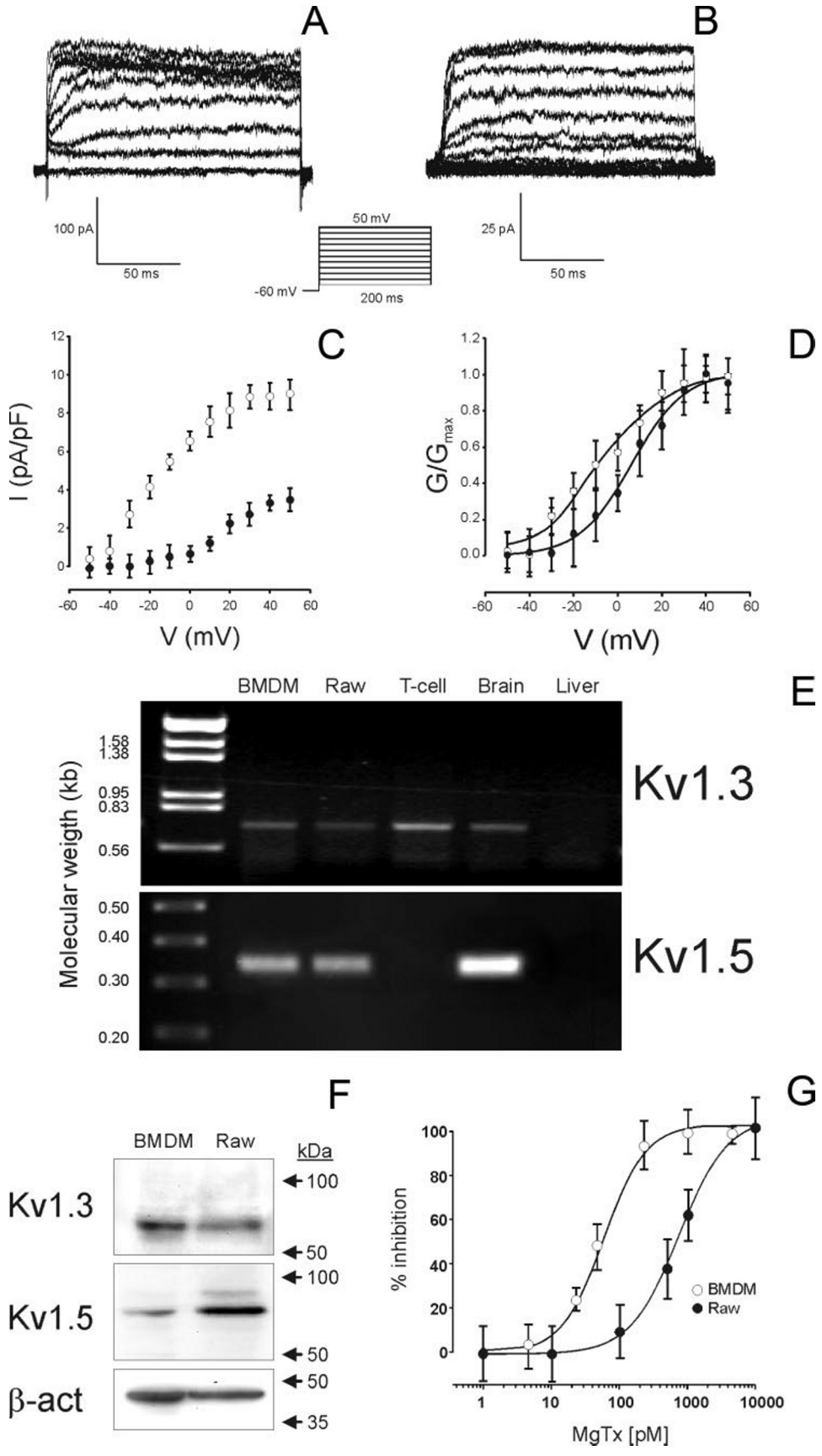
A
B
100 pA
50 ms
50 mV
-60 mV
200 ms
25 pA
50 ms
C
I (pA/pF)
V (mV)
D
G/G$_{max}$
V (mV)
E
BMDM
Raw
T-cell
Brain
Liver
Molecular weigth (kb)
1.58
1.38
0.95
0.83
0.56
Kv1.3
0.50
0.40
0.30
0.20
Kv1.5
F
BMDM
Raw
kDa
Kv1.3
100
50
Kv1.5
100
50
β-act
50
35
G
% inhibition
BMDM
Raw
MgTx [pM]

maximal conductance G_{max}. G/G_{max} was plotted *versus* V_h. The normalized G/G_{max} *versus* voltage curve was fitted using the Boltzmann equation, $G/G_{max} = 1/(1 + \exp^{((V_{½} - V)/k)})$, where $V_{½}$ is the voltage at which the current is half-activated, and k is the slope factor of the activation curve. To calculate inactivation time, constants (τ) cells were held at −60 mV, and pulse potentials of 4 s were applied. Inactivation adjustment was calculated from the peak of the current at 50 mV to the steady-state inactivation, and traces were fitted with Sigma Plot (SPSS Inc.). To analyze the cumulative inactivation, currents were elicited by a train of 8 depolarizing voltage steps of 200 ms to + 50 mV once every 400 ms.

Oocytes were voltage-clamped with a two-electrode system, Gene Clamp 500 (Axon Instruments). The voltage and the current microelectrodes were filled with KCl (3 M) and had resistances ranging from 0.5 to 1 megaohms. The volume of the oocyte recording chamber was 200 μl. Recordings were done under constant bath perfusion (1 ml/min). The bath electrode was an Ag-AgCl pellet that made contact with the recording solution (115 mM NaCl, 2 mM KCl, 1.8 mM $CaCl_2$, and 10 mM HEPES at pH 7.4) through an agar bridge. Membrane potential and current were digitized through a PCI-MIO-16E-4 Multifunction I/O Board and NI-DAQ (National Instruments). The board was controlled by the Whole Cell Analysis Program (kindly provided by John Dempster, University of Strathclyde). The signal was filtered at twice the acquisition frequency. Oocytes were clamped to a holding potential of −60 mV. To evoke voltage-gated currents, all oocytes were stimulated with 1-s square pulses ranging from −80 mV to +80 mV in 10-mV steps. To ensure complete recovery from inactivation, oocytes were repolarized for 60 s at −60 mV. To calculate inactivation time constants (τ), pulse potentials of 5 s were applied. Inactivation adjustment was calculated from the peak of the current at + 80 mV to the steady-state inactivation, and traces were fitted with Sigma Plot (SPSS Inc.). Data were leak-subtracted using hyperpolarizing P/4 subtraction pulses. Data were analyzed by the Whole Cell Analysis program.

To characterize the voltage-dependent outward K^+ current pharmacologically, recombinant margatoxin (MgTx) was added to the external solution (8, 11). Toxin was reconstituted at 10 μM in Tris buffer (0.1% bovine serum albumin, 100 mM NaCl, 10 mM Tris, pH 7.5). Solutions were perfused by gravity and controlled by electrovalves (ALA, Scientific Instruments). All recordings were performed at room temperature (20–23 °C).

Statistics—Values are expressed as the mean ± S.E. The significance of differences was established by Student's *t* test or by analysis of variance (GraphPad, PRISM 4.0) where indicated. A value of $p < 0.05$ was considered significant.

RESULTS

Macrophages Express Kv1.3 and Kv1.5 Channels—Voltage-dependent potassium currents were evoked in macrophages by depolarizing pulses. Fig. 1, *A* and *B*, show representative potassium currents in BMDM and Raw 264.7 macrophages, respectively. The current density (picoamperes/picofarads)/voltage relationships depicted in Fig. 1*C* indicate that currents in BMDM were 3-fold higher than in Raw cells. Fig. 1*D* shows the normalized conductance against the test potential. Although the threshold for activation was about −40 mV in BMDM, channels opened at −20 mV in Raw macrophages. Whereas k slopes were similar for both groups (18.3 ± 3 and 11.9 ± 2 for BMDM and Raw, respectively, $n = 10$), $V_{½}$ values were significantly different (−7.2 ± 2 and 6.3 ± 2 mV for BMDM and Raw, respectively, $p < 0.001$, $n = 10$).

Kv1.3 is the main voltage-dependent K^+ channel in leukocytes (2). This was confirmed by RT-PCR analysis in our cells. Fig. 1*E* shows that not only EL-4, a murine T-cell line, but also macrophages (BMDM and Raw) expressed Kv1.3. However, the presence of Kv1.5 was only observed in macrophages. Mouse brain and liver RNAs were used as positive and negative controls, respectively. The presence of Kv1.5 protein in both myeloid cell lines was further confirmed by Western blot analysis performed in crude membrane preparations (Fig. 1*F*).

Contrary to Kv1.5, Kv1.3 is highly sensible to specific toxins (21). K^+ currents in BMDM are blocked by Kv1.3 inhibitors such as MgTx and ShK-Dap^{22} (8, 11). However, the presence of Kv1.5 indicates that either Kv1.5 forms homotetrameric complexes or Kv1.5 subunits are assembled with Kv1.3 in heterotetrameric structures that are sensitive to Kv1.3 toxins. Fig. 1*G* shows that K^+ currents in both macrophage cell lines are inhibited by the presence of MgTx. The IC_{50} values were 50 ± 5.1 and 772 ± 40 pM for BMDM and Raw, respectively ($p < 0.001$, $n = 10$). MgTx does not block Kv1.5 (21). Therefore, these results indicate that, although Kv1.5 is expressed, this subunit does not form homomeric channels in macrophages. However, Raw and BMDM may differ in the K^+ channel complex composition since biophysical and pharmacological differences were evident.

Co-localization experiments supported the pharmacological and biophysical data. Unfortunately, immunocytochemistry studies with anti-Kv1.3 and anti-Kv1.5 antibodies were unsuccessful, probably due to high levels of Fc receptors expressed in macrophages. However, since Raw cells have the different Kv1.3 and Kv1.5 intracellular processing and trafficking programs, we transfected these cells with Kv1.3-YFP and Kv1.5-CFP. In general, cells were poorly transfected, but confocal analysis of double-transfected Raw cells demonstrated that Kv1.5 co-localized with Kv1.3 at the macrophage plasma mem-

FIGURE 1. **Macrophages express voltage-dependent K^+ channels.** Shown are representative traces of K^+ currents evoked in BMDM (*A*) and Raw 264.7 macrophages (*B*). Cells were held at −60 mV, and currents were elicited by depolarizing pulses in 10-mV steps (200-ms duration) from −50 to +50 mV. To ensure completely recovery from inactivation, cells were repolarized for 45 s at −60 mV. *C*, current density *versus* voltage relationship of K^+ currents. *D*, normalized conductance plotted *versus* voltage. *E*, mRNA expression of Kv1.3 and Kv1.5. Raw, Raw 264.7 cells; T-cell, EL-4 T-lymphocytes. 1 μg of total RNA was used in RT-PCR reactions, as described under "Experimental Procedures." *kb*, kilobases. *F*, Kv1.3 (67 kDa) and Kv1.5 (90 and 74 kDa) protein expression in BMDM and Raw 264.7 macrophages. *G*, dose-dependent inhibition curves of the K^+ current by MgTx. Currents were evoked at +50 mV from a holding potential of −60 mV during a pulse potential of 200 ms. The percentage inhibition was calculated by comparing the current at a given concentration of toxin *versus* that obtained in its absence. Symbols for *panels C*, *D*, and *G* are: ○, BMDM; ●, Raw 264.7 macrophages. Values are the mean ± S.E.

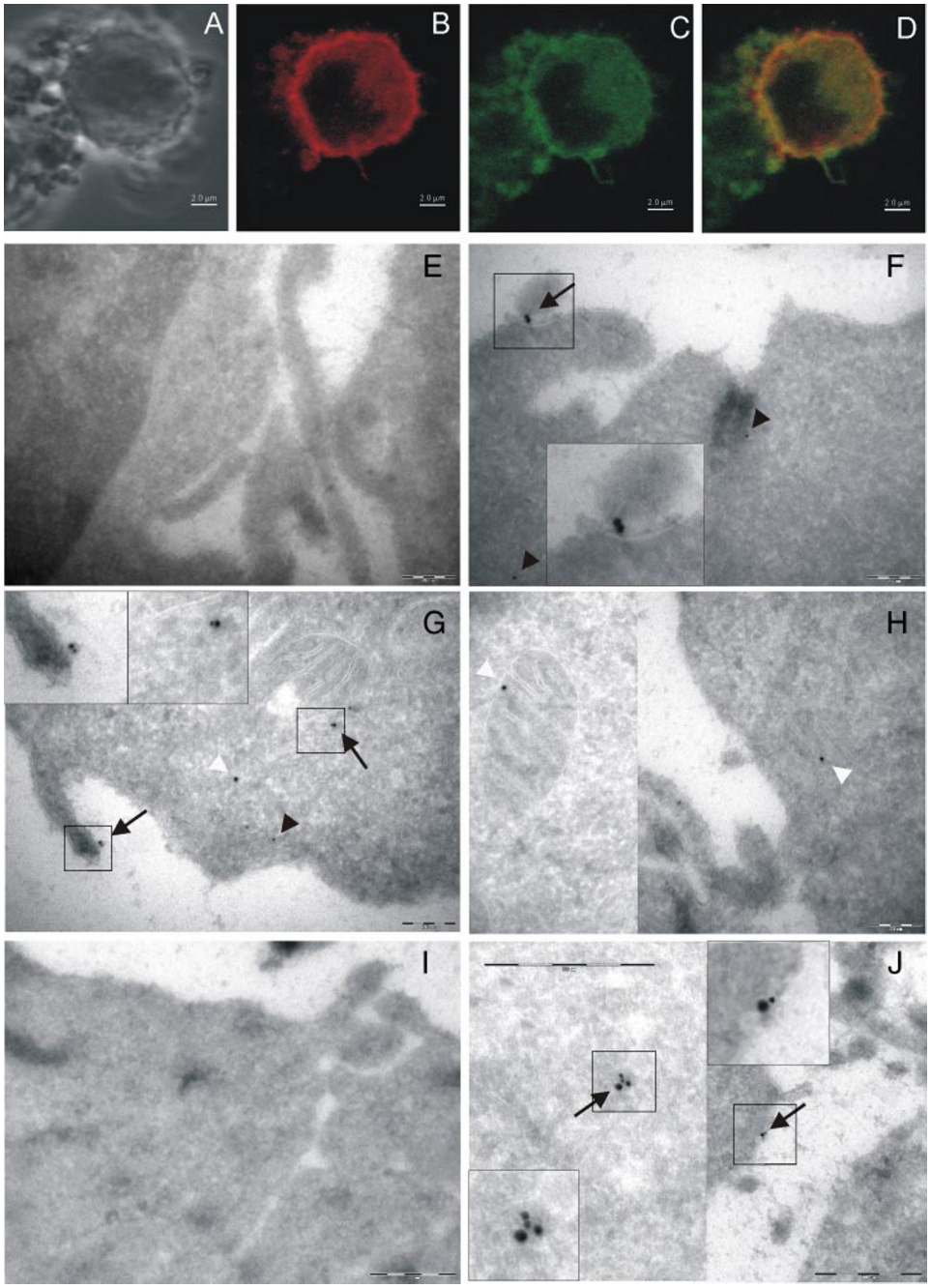

FIGURE 2. **Kv1.3 and Kv1. 5 co-localize at the macrophage membrane.** Shown is confocal imaging of Kv1.3-YFP and Kv1.5-CFP co-transfected Raw 264.7 cells. *A*, phase image of a Raw macrophage. Kv1.3-YFP (*B*) and Kv1.5-CFP (*C*) are expressed on the cell surface. *D*, overlay of the two images demonstrating co-localization of both proteins at the macrophage membrane. *Bars* indicate a 2-μm scale. *Panels E–J*, electron microscopy of Kv1.3 (15-nm gold) and Kv1.5 (10-nm gold) in non-transfected Raw 264.7 (*E–H*) and HEK-293 (*I–J*) cells. *E*, negative control using secondary antibodies. *F*, Raw cells expressing Kv1.3 and Kv1.5. *G*, hybrid channel detection. *H*, Kv1.3 channel detection at mitochondria. *I–J*, HEK cells transfected with Kv1.3 and Kv1.5. *I*, negative control using secondary antibodies. *J*, hybrid channel detection. *Bars* indicate 200 nm and 500 nm in Raw and HEK cells, respectively. *Boxes* are magnified for detail. *Black arrowhead*, Kv1.5; *white arrowhead*, Kv1.3; *arrows*, homo- and heteromeric channels.

brane (Fig. 2, *A–D*). In this context heteromeric channels could be immuno-detected by electron microscopy. Using this approach we detected oligomeric complexes both at the membrane and inside the cell (Fig. 2, *E–H*). Interestingly, some immunogold staining was also present at mitochondria (Fig. 2*H*), in which Kv1.3 has been previously described (22). Although a similar heteromeric pattern was obtained in double-transfected HEK cells (Fig. 2, *I* and *J*), no Kv1.5 immunogold labeling was observed in HEK cells expressing homomeric Kv1.3 channels (data not shown).

Kv1.3 and Kv1.5 Form Functional Heterotetrameric Kv Channels in HEK-293 Cells—If heterotetramer formation occurs in macrophages, the electrophysiological and pharmacological profiles of heterologously expressed hybrid channels should be consistent with those present in native cells. To explore this hypothesis, we studied the expression of Kv1.3 and Kv1.5 in HEK-293 cells (Fig. 3). We first analyzed whether our constructs were fully functional and generated K^+ currents. Fig. 3, *A–C*, shows that HEK cells transfected with Kv1.3-YFP evoked K^+ currents. Similar results were obtained with Kv1.5-CFP (Fig. 3, *D–F*). In addition, Kv1.3 and Kv1.5 co-localized in double-transfected HEK cells, and as a result, K^+ currents were a mixture of those generated by homomeric channels (Fig. 3, *G–J*). Although the threshold voltage for activation was about -40 mV in homomeric Kv1.3 and hybrid Kv1.3/Kv1.5 channels, in Kv1.5 channels it was -20 mV. Plots of normalized conductance against membrane potential for Kv1.3-, Kv1.5-, and Kv1.3/Kv1.5-expressing cells are shown in Fig. 3*K*. Although $V_{½}$ values were -23.6 ± 0.9 and -6.7 ± 0.7 mV for Kv1.3 and Kv1.5, respectively, the heterotetramer showed a half-activation voltage of -20.1 ± 1.2 mV. Furthermore, k slope values were 10.6 ± 1, 7.2 ± 1, and 10.7 ± 1 for Kv1.3, Kv1.5, and the Kv1.3/Kv1.5 heterotetramer, respectively ($n = 10$).

Although Kv1.5 is resistant to MgTx, both homomeric Kv1.3 and heterotetrameric Kv1.3/Kv1.5 channels are highly sensitive to this toxin (Fig. 3, *L* and *M*). However, although Kv1.3 was inhibited with an IC_{50} of ~336 pM, hybrid Kv1.3/Kv1.5 channels were fully blocked but were much less sensitive to MgTx ($IC_{50} \sim 25$ nM). As observed in macrophages (see above), sensitivity to the toxin indicates that Kv1.5 is not expressed as a homomultimeric channel in HEK cells rather than forming heteromeric complexes with Kv1.3. The characteristic C-type inactivation of Kv1.3 is absent in Kv1.5 (21, 23).

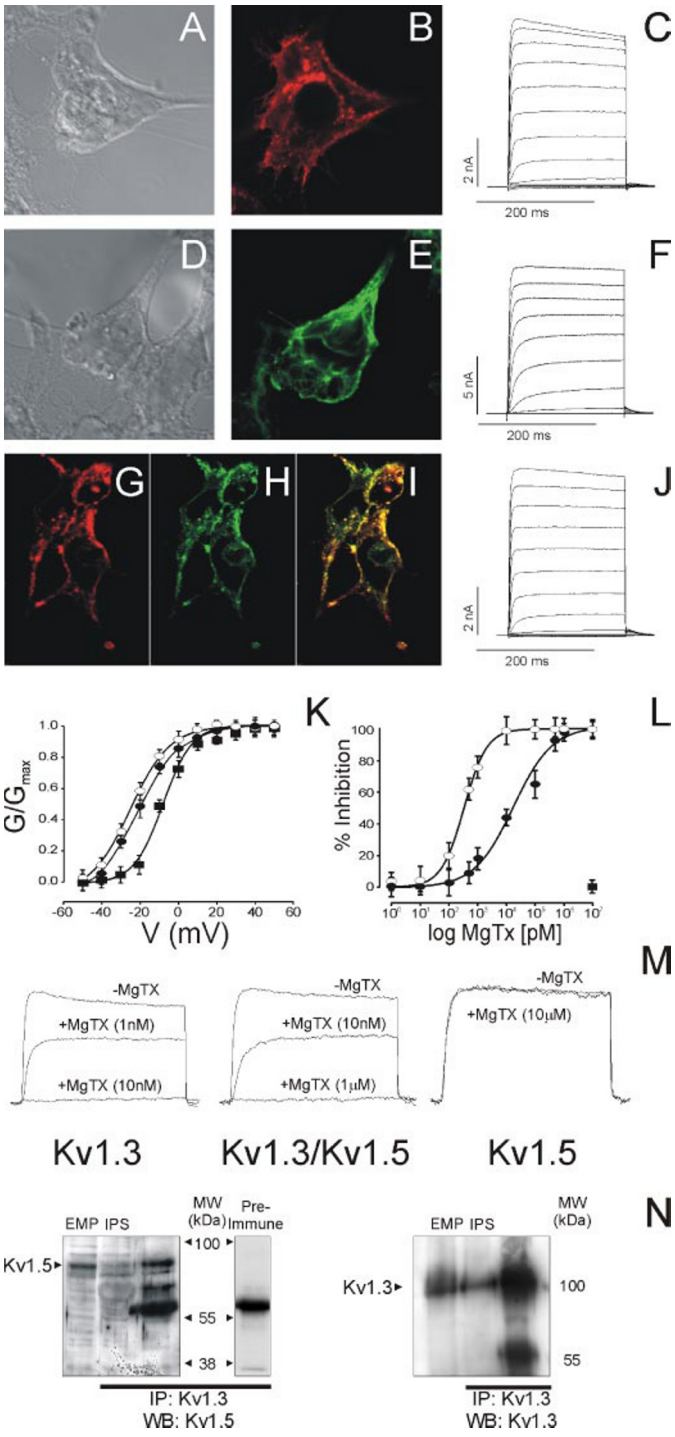

FIGURE 3. **Kv1.3 and Kv1. 5 heterotetramers are functional voltage-dependent potassium channels when expressed in HEK-293 cells.** *A–C*, Kv1.3-YFP generates K^+ currents. *A*, phase image of a representative HEK cell. *B*, a confocal image demonstrating that the Kv1.3 channel targets the membrane. *C*, outward-delayed rectifier K^+ currents in Kv1.3-YFP transfected cells. *D–F*, Kv1.5-CFP also generates K^+ currents when expressed in HEK-293 cells. *D*, phase micrograph of a HEK cell. *E*, expression of Kv1.5-CFP. *F*, outward-delayed rectifier K^+ currents in Kv1.5-CFP transfected cells. *G–J*, Kv1.3-YFP and Kv1.5-CFP co-localize in doubly-transfected HEK cells. *G*, Kv1.3-YFP. *H*, Kv1.5-CFP. *I*, overlay of the two images. *Yellow* signifies co-localization. *J*, K^+ currents generated in doubly transfected HEK cells. To evoke K^+ currents, HEK cells were held at −60mV, and pulse potentials were applied as described in Fig. 1. *K*, plot of normalized conductance *versus* test potential. Conductance was normalized to the peak current at +50 mV. *L*, dose-dependent inhibition curves of the K^+ current by MgTx. Peak currents were evoked at +50 mV, and the percentage inhibition was calculated as described in Fig. 1. *M*, representative normalized traces obtained upon depolarization from −60 mV to +50 mV of Kv1.3 (*left*), Kv1.3/Kv1.5 (*center*), and Kv1.5 (*right*) expressed in HEK cells. After establishing the patch clamp configuration, currents were evoked at +50 mV. MgTx was further added to the bath chamber, and recordings were obtained after 1 min. Symbols for *panels K* and *L* are: ○, Kv1.3; ●, Kv1.3/Kv1.5; ■, Kv1.5. Values are the mean ± S.E. *N*, Kv1.3 and Kv1.5 co-associate in HEK cells. Immunoprecipitation experiments were performed in doubly transfected cells. Enriched membrane preparations (*EMP*) were immunoprecipitated (*IP*) with anti-Kv1.3 antibodies. The starting material (enriched membrane preparations (*EMP*) and the immune-precipitated supernatant (*IPS*) were further immunoblotted with anti-Kv1.5. Immunoprecipitates (*IP*) with anti-Kv1.3 were immunoblotted (*WB*) with anti-Kv1.3, anti-Kv1.5 serum and preimmune serum.

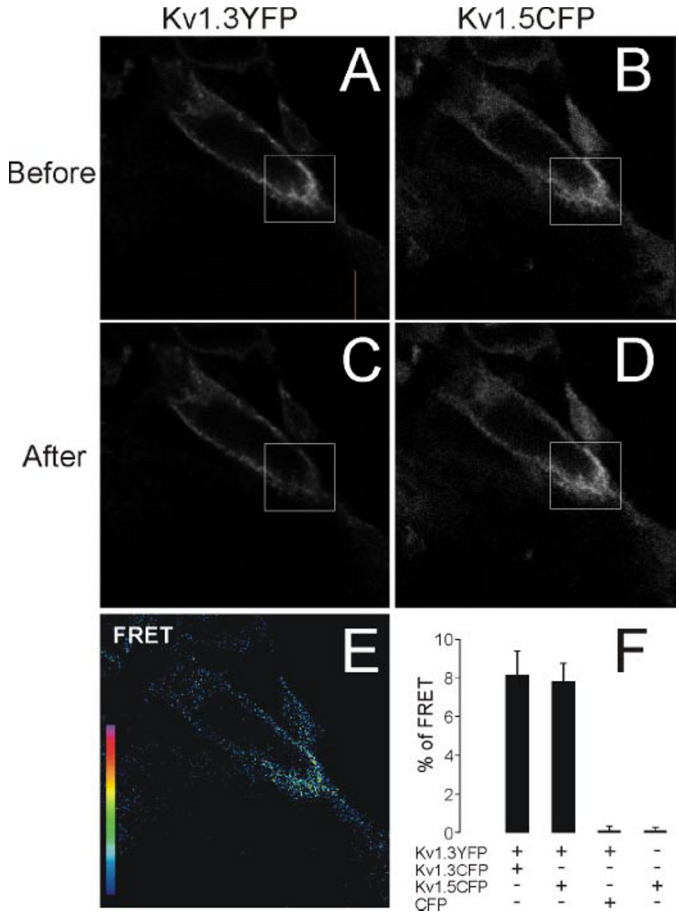

FIGURE 4. **Molecular association of Kv1.3 and Kv1.5. HEK cells were doubly transfected with Kv1.3-YFP and Kv1.5-CFP, and FRET was performed.** A representative experiment is shown. *A–D*, fluorescence signal of Kv1.3-YFP and Kv1.5-CFP before (*A* and *B*) and after (*C* and *D*) photobleaching of YFP, respectively. The region studied is delimited by the *box*. *E*, FRET panel representing the difference in CFP fluorescence intensity before and after photobleaching. *F*, FRET efficiency of different combinations. Kv1.3-YFP/Kv1.3-CFP was used as a positive control. Negative controls were performed with cells expressing Kv1.3-YFP/CFP and Kv1.5-CFP alone.

Thus, the presence of the latter in MgTx-sensible hybrid channels increased the time constant of inactivation in HEK cells (555 ± 40 ms and 832 ± 100 ms for Kv1.3 and Kv1.3/Kv1.5 at +50 mV, respectively, $p < 0.05$), further demonstrating heteromeric Kv1.3/Kv1.5 association. In addition, panels on Fig. 3*N* show that, although the immunoprecipitation with anti-Kv1.3 antibody was not fully effective, Kv1.5 co-immunoprecipitated with Kv1.3 in double-transfected HEK cells. Thus, confocal imaging, immunoprecipitation, and immunogold detection by electron microscope (see Fig. 2*J*) indicated that Kv1.3 and Kv1.5

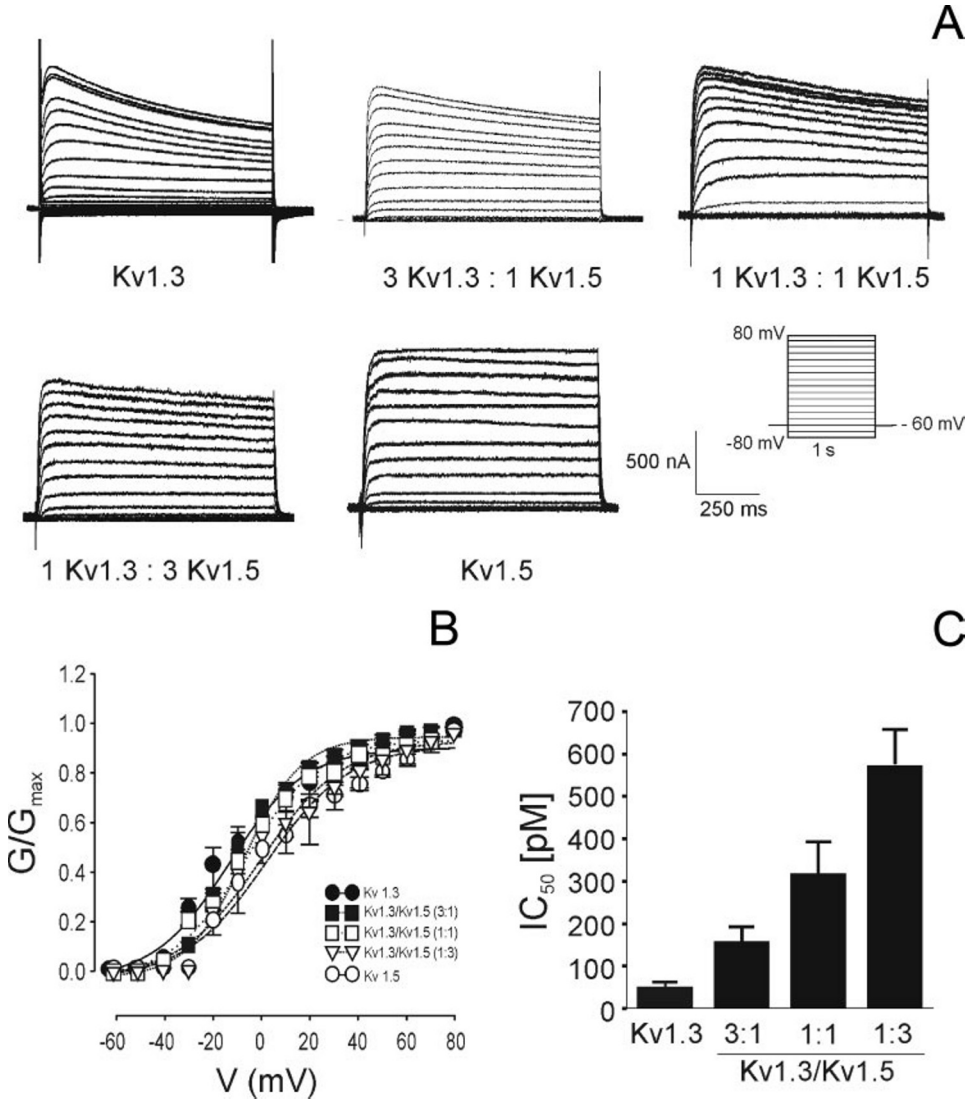

FIGURE 5. **Expression of different ratios of Kv1.3 and Kv1.5 in *Xenopus* oocytes.** *A*, representative traces of K^+ currents evoked in oocytes injected with different ratios of Kv1.3 and Kv1.5. Pulse protocols are shown. To ensure complete recovery from inactivation, cells were repolarized for 60 s at −60 mV. Maximum conductance values (+80 mV) were always between 5 and 10 microsiemens, with a mean of 9.3 ± 2.2 microsiemens. *B*, plot of normalized conductance against test potential. *C*, IC_{50} for margatoxin-sensitive K^+ currents in homo- (Kv1.3) and various heterotetrameric (Kv1.3/Kv1.5) channels. Currents were evoked at +80 mV from a holding potential of −60 mV during a pulse potential of 1 s. Values are mean ± S.E. of at least five independent oocytes.

co-localized at the membrane and co-assembled, forming a functional heteromeric complex. However, to further confirm this physical association, we undertook FRET analysis (Fig. 4). A confocal section of doubly labeled cells before photobleaching is shown in *panels A* and *B*. Once the long-wavelength fluorescence of the acceptor was eliminated (*panel C*), the donor intensity was measured again (*panel D*), and FRET efficiency was calculated (*panels E* and *F*). The mean FRET efficiency of homotetrameric Kv1.3 channels (Kv1.3-CFP/Kv1.3-YFP) indicated an increment significantly greater than 0% (8%). Similar results were obtained with hybrid Kv1.3/Kv1.5 channels. However, neither Kv1.3-YFP with CFP nor Kv1.5-CFP gave FRET efficiency different from 0%. Our results confirm molecular proximity between Kv1.3 and Kv1.5, as reported by co-immunoprecipitation, co-localization, and electron microscopy.

Heteromultimeric Assembly of Kv1.3 and Kv1.5 in Xenopus Oocytes—To analyze heterotetrameric compositions of the functional Kv complex, we injected several ratios of cRNA from Kv1.3 and Kv1.5 into *Xenopus* oocytes. Oocytes were divided into 5 groups and injected with Kv1.3 (10 ng), Kv1.5 (10 ng), or various ratios of Kv1.3 and Kv1.5 (final amount 10 ng). Fig. 5 shows representative traces of all groups. Membrane currents in oocytes injected with Kv1.3 or Kv1.5 alone were essentially the same as those previously described (9, 24). Similar to that observed in HEK cells, homomeric Kv1.3 generated a delayed rectifier K^+ channel with a moderate degree of inactivation (Fig. 5*A*). However, depolarizing pulses in Kv1.5-injected oocytes evoked a non-inactivating K^+ current. Co-expression of Kv1.3 and Kv1.5 resulted in voltage-dependent K^+ currents with properties distinct from those of homomultimeric channels. Increasing concentrations of Kv1.5 range from currents very similar to homomeric Kv1.3 (3 Kv1.3:1 Kv1.5) to resemble Kv1.5 alone (1 Kv1.3: 3 Kv1.5). The steady-state activation of K^+ currents is depicted in Fig. 5*B*. Normalized conductances demonstrated that, whereas in homomeric Kv1.3 or high ratios of Kv1.3 channels the threshold voltage for activation ranged from −40 to −30 mV, in either Kv1.5 or high ratios of Kv1.5 channels threshold voltage was about −20 mV. Increasing concentrations of Kv1.5 shifted the half-activation voltage to more positive potentials. Thus, $V_{½}$ values were −11.3 ± 3, −9.8 ± 1, −6.4 ± 2, 0.1 ± 3, and 2 ± 3 mV for Kv1.3, hybrids Kv1.3/Kv1.5 (3:1, 1:1, 1:3), and Kv1.5, respectively ($p <$ 0.001, analysis of variance). In addition, k slope values were almost similar in all groups, 15.6 ± 2, 11.8 ± 1, 15.2 ± 2, 17.1 ± 3, and 16.9 ± 9 for Kv1.3, hybrids Kv1.3/Kv1.5 (3:1, 1:1, 1:3), and Kv1.5, respectively. Pharmacological studies indicate that, similar to what was observed in HEK cells, the presence of Kv1.5 led to less MgTx-sensitive K^+ currents (Fig. 5*C*). Thus, higher IC_{50} were obtained as a result of increasing Kv1.5 ratios, which were 47 ± 10 (Hill coefficient 1.1), 153 ± 40 (Hill coefficient 0.51), 313 ± 80 (Hill coefficient 0.54), and 568 ± 90 (Hill coefficient 0.54) pM for Kv1.3 and hybrids Kv1.3/Kv1.5 (3:1, 1:1, 1:3), respectively ($p < 0.001$, analysis of variance). Finally, the time constant of inactivation at +80 mV also increased and were

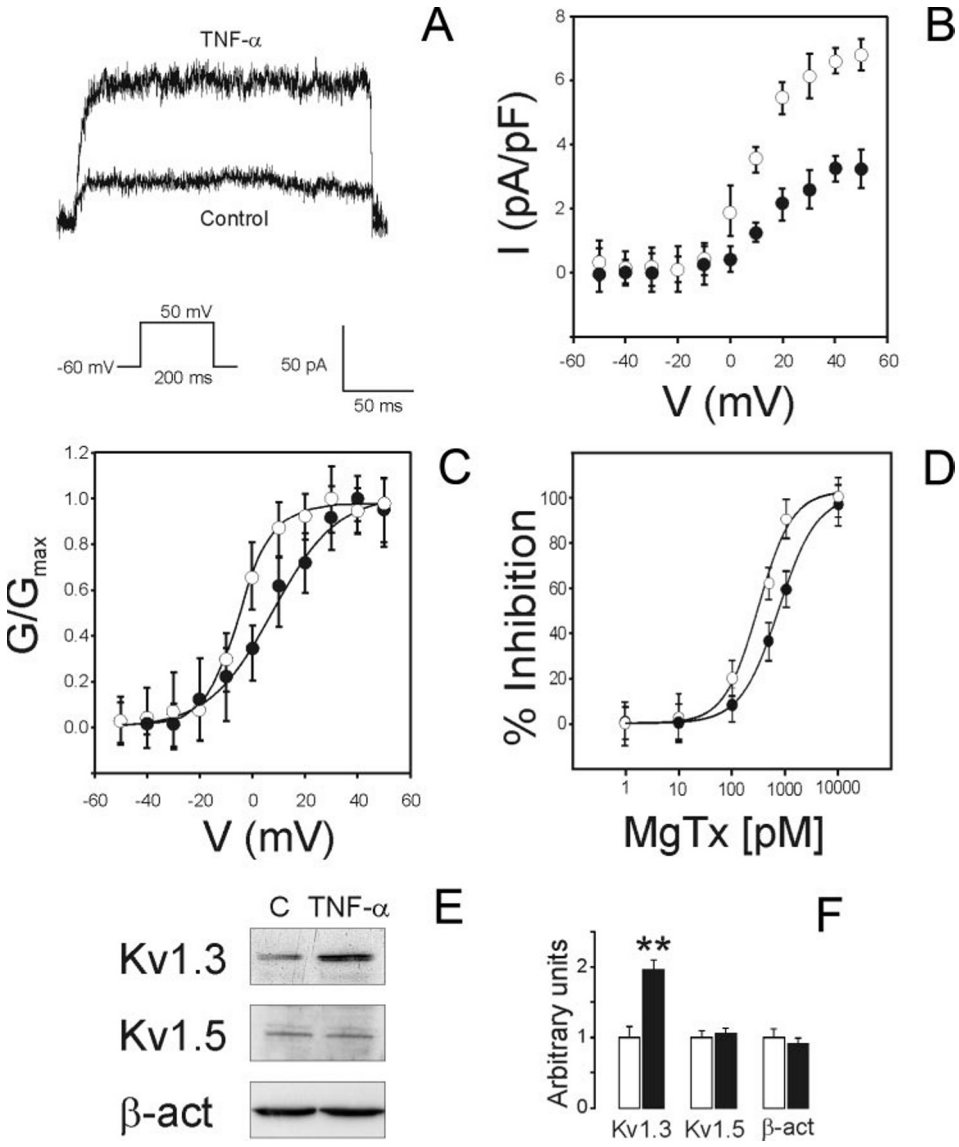

FIGURE 6. **TNF-α differentially regulates Kv1.3 and Kv1.5 concomitantly to biophysical and pharmacological changes of K^+ currents in Raw 264.7 macrophages.** Cells were incubated for 24 h in the presence or absence of TNF-α. *A*, representative traces of K^+ currents elicited by a +50-mV depolarizing pulse (200 ms) in control and TNF-α-treated Raw cells. *B*, current density *versus* voltage relationship of K^+ currents. *C*, normalized conductance plotted against test potential. *D*, dose-dependent inhibition curves of the K^+ current by MgTx. Currents were evoked, and the percentage inhibition was calculated as described in Fig. 1. Symbols in *panels B–D* are: ●, control; ○, TNF-α. *E*, Kv1.3 and Kv1.5 Western blot analysis of enriched membrane preparations from Raw macrophages in the absence (*Control*) or the presence (*TNF-α*) of the cytokine. Representative blots are shown. *β-act*, β-actin. *F*, Kv1.3 and Kv1.5 protein expression values derived from *panel E*. In all cases arbitrary units are standardized to the control value in the absence of TNF-α. *Open bars*, control; *closed bars*, TNF-α. Values are the mean ± S.E. of at least three independent experiment. **, $p < 0.01$ *versus* control (Student's *t* test).

526 ± 50, 833 ± 70, 963 ± 50, 1470 ± 250, and >5000 ms for Kv1.3, hybrids Kv1.3/Kv1.5 (3:1, 1:1, 1:3), and Kv1.5, respectively ($p < 0.001$, analysis of variance).

Kv heteromeric Composition Changes in Macrophages Altering Pharmacology and Biophysics—Our results have physiological significance because Kv channels in leukocytes are considered pharmacological targets, and the composition of the channel complex could impair potential therapies. Thus, differential regulation of Kv1.3 and Kv1.5 could modify the subunit composition of the channel, altering the biophysical and pharmacological properties. To ascertain this, we cultured Raw macrophages in the presence of TNF-α (Fig. 6). This cytokine, produced by leukocytes under a systemic inflammatory response, activates macrophages and regulates Kv (8, 25). The addition of TNF-α for 24 h increased outward-delayed rectifier K^+ currents up to 3-fold. Half-activation voltage shifted to negative potentials (7.9 ± 1.6 and −6.8 ± 1.5 mV for control and TNF-α, respectively, $p < 0.001$, $n = 30$), and k slope values were different (11.5 ± 1.3 and 6.5 ± 1.2 for control and TNF-α, respectively, $p < 0.001$, $n = 30$). In addition, whereas this cytokine induced Kv1.3 protein expression, Kv1.5 abundance remained constant. Other functional parameters also support an increase of Kv1.3 subunits in TNF-α-activated cells. Thus, an ~10-mV hyperpolarized shift in the membrane potential (data not shown) and a decrease of the IC_{50} for Margatoxin (772 ± 40 and 319 ± 48 pM, $p < 0.001$) were observed in cells treated with the cytokine. Because Kv1.3 is involved in macrophage activation (8, 10), our results are consistent with an increased number of Kv1.3 subunits, either as homomeric Kv1.3 or hybrid Kv1.3/Kv1.5 channels.

TNF-α-induced activation as well as the differential expression of Kv1.3 and Kv1.5 in different cell types modifies the Kv1.3/Kv1.5 ratio, altering the cellular excitability and leading to functional consequences. High Kv1.3/Kv1.5 ratios, as observed in BMDM and TNF-α-activated Raw cells (Fig. 7*A*), are in agreement with more hyperpolarized half-activation voltages, rapid inactivation time constants, more cumulative inactivation, and lower IC_{50} for MgTx (Fig. 7, *B–E*). However, low Kv1.3/Kv1.5 ratios as observed in control Raw cells would modify kinetics and alter pharmacology.

DISCUSSION

This study demonstrates that Kv1.3 and Kv1.5 can form heterotetrameric structures and suggests that Kv1.3/Kv1.5 hybrid K^+ channels contribute to the major Kv channel in macrophages. Furthermore, our data also show that the Kv1.3/Kv1.5 ratio may vary in the Kv complex, leading to biophysically and pharmacologically distinct channels.

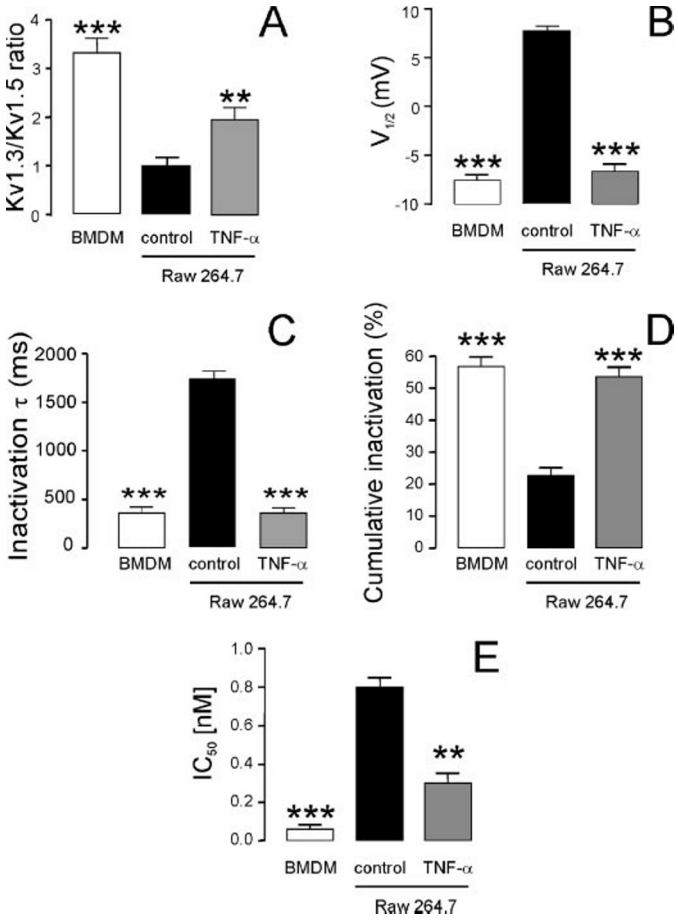

FIGURE 7. **Variations in the Kv1.3/Kv1.5 ratio are correlated with changes in biophysical and pharmacological properties of K^+ currents in macrophages.** *A*, Kv1.3/Kv1.5 ratios in BMDM and Raw cells cultured in the presence or the absence of TNF-α were calculated from Western blots similar to those shown in Figs. 1 and 6 and standardized to the value of control Raw 264.7 cells. Values are the mean ± S.E. of at least three independent experiments. *B*, half-activation voltage of K^+ currents in macrophages. Values were calculated from steady-state activation curves of the outward current. Conductance was normalized to the peak current at +50 mV. *C*, time constant of inactivation (τ). Cells were held at −60 mV, and a + 50 mV pulse potential was applied during 4 s. *D*, percentage of cumulative inactivation. Currents were elicited by a train of 8 depolarizing voltage steps of 200 ms to +50 mV once every 400 ms. The percentage was calculated as a result of the difference between the peak current at the first pulse and the remaining current at the last. *E*, IC_{50} values of the K^+ current in the presence of MgTx. Currents were evoked, and the percentage inhibition was calculated as described in Fig. 1. *Open bars*, BMDM; *closed bars*, control Raw 264.7 cells; *gray bars*, TNF-α-activated Raw 264.7 cells. **, $p < 0.01$; ***, $p < 0.001$ *versus* control (Student's *t* test).

Although heteromeric structures between either Kv1.3 or Kv1.5 and other Kv1 subunits had been described (7, 26–29), our study demonstrates for the first time that Kv1.3 assembles with Kv1.5 to generate functional Kv complexes. Thus, similar to nerve and muscle, in macrophages it is difficult to assign currents to specific channels. Tissue localization and the absence of currents other than those generated by homomeric channels argue against certain Kv complexes (30–32). Thus, the assembly of Kv1.3 with Kv1.1 and Kv1.2 was questioned by immunohistochemical localization in mouse rod bipolar cells (30). In addition, a differential distribution also argues against a heteropolymer between Kv1.1 and Kv1.5 in Schwann cells (31). In contrast, Kv1.5 co-assembles with Kv1.2 and Kv1.4 in GH3 pituitary cells, brain cortex, and the cardiovascular system (7, 17, 26). However, in GH3 cells, up to 70% of the channels were pharmacologically identified as Kv1.5 homomers (17). This is not the case in murine macrophages, since the presence of Kv1.5 in heterotetrameric Kv1.3/Kv1.5 channels induced a shift to positive potentials concomitantly with a loss of sensitivity to MgTx. Unlike Kv1.5, Kv1.3 and hybrids Kv1.3/Kv1.5 are highly sensitive to MgTx. Our data argue against homotetrameric channels consisting of Kv1.5, but the presence of Kv complexes generated only by Kv1.3 cannot be ruled out.

Kv1.3 subunit is the main responsible for outward-delayed rectifier potassium currents in leukocytes (2). Nonetheless, although half-activation voltages of Kv1.3 currents in T-cells range from −14 to −35 mV, $V_{½}$ values are more depolarized in BMDM and Raw macrophages (Refs. 8 and 11 and this study). Unlike T-cells, macrophages express Kv1.5, which shows more positive potentials when expressed in heterologous expression systems (10). In brain macrophages, a switch from Kv1.5 to Kv1.3 during cell growth was described, and the half-activation voltage of the Kv currents was shifted ~17 mV to hyperpolarized values in proliferating cells (10). This is similar to what we found in BMDM and TNF-α-activated Raw cells, where negative shifts could be caused by higher Kv1.3/Kv1.5 ratios. In this scenario, pharmacological and gating parameters in oocytes expressing different Kv1.3/Kv1.5 ratios support the contribution of different heteropolymeric complexes to the major Kv in BMDM and Raw macrophages. Whereas BMDM exhibit $V_{½}$ and IC_{50} values similar to Kv1.3 homo and Kv1.3/Kv1.5 (3:1) heterotetrameric structures, Raw macrophages were more like Kv1.3/Kv1.5 (1:1 or 1:3).

A change in the Kv1.3/Kv1.5 ratio in the Kv complex would affect kinetic parameters and pharmacology. Because TNF-α induces differential regulation of K^+ channels (8, 11, 25), our results are consistent with the possibility that the cytokine alters the stoichiometry of the subunits in the channel. In addition, a new composition could also affect the interaction with the Kvβ subunits in macrophages, thus modifying the gating kinetics (11). Association or lack of association with endogenous β-subunits could also affect the phenotype of the resulting current. Our data show that potassium channels from activated cells are more sensitive to small changes in the membrane potential. Thus, these cells would be more excitable at negative potentials. In this context it has been described that a depolarizing change of +25 mV modifies IL-2 production, thus reducing the activation and antibody production of lymphocytes (34). Hormones and cytokines may produce long-term effects on excitability by regulating K^+ channel gene expression. Although Kv1.3 expression is induced during activation and apoptosis, down-regulation is associated with immunosuppression (18). Dexamethasone, a glucocorticoid antagonist, induces Kv1.5 expression in pituitary cells and cardiomyocytes and inhibits Kv1.3 in T-cells (16–18). Panyi *et al.* (35, 36) located Kv1.3 in the immunological synapse between cytotoxic and target cells. Activating cytokines would increase the amount of Kv1.3 subunits, forming either homo- or heterotetrameric structures, and changes in Kv composition would modify membrane excitability within the immunological synapse between T-lymphocytes and macrophages. Thus, hormones

and cytokines can affect the expression of cell surface homomeric and heteromeric channels in different ways, leading to specific alteration of excitability.

In summary, our results demonstrate that Kv1.3 and Kv1.5 form heterotetrameric K^+ channels in macrophages. In addition, the physiological regulation of the Kv channel subunit stoichiometry may be an important mechanism triggering the specific immune response. The findings of the present study are of interest since K^+ channels in leukocytes are considered pharmacological targets in autoimmune diseases (33), and as we demonstrate, different channel composition may change biophysical properties and alter the use of potential drug therapies. Macrophages present antigens to infiltrating T-lymphocytes, and the predominance of Kv1.3 in activated macrophages could generate more specific drug-sensitive complexes leading to more effective therapies.

Acknowledgments—We thank L. Martín and J. Bertrán for help with macrophage cultures. The editorial assistance of the Language Advisory Service from the University of Barcelona is also acknowledged.

REFERENCES

1. Hille, B. (2001) *Ion Channels of Excitable Cells*, 3rd Ed., Sinauer Associates, Sunderland, MA
2. Cahalan, M. D., Wulff, H., and Chandy, K. G. (2001) *J. Clin. Immunol.* **21,** 235–252
3. Martens, J. R., Kwak, Y. G., and Tamkun, M. M. (1999) *Trends Cardiovasc. Med.* **9,** 253–258
4. MacKinnon, R. (1991) *Nature* **350,** 232–235
5. Isacoff, E. Y., Jan, Y. N., and Jan, L. Y. (1990) *Nature* **345,** 530–534
6. Wang, F. C., Parcej, D. N., and Dolly, J. O. (1999) *Eur. J. Biochem.* **263,** 230–237
7. Po, S., Roberds, S., Snyders, D. J., Tamkun, M. M., and Bennett, P. B. (1993) *Circ. Res.* **72,** 1326–1336
8. Vicente, R., Escalada, A., Coma, M., Fuster, G., Sanchez-Trillo, E., Lopez-Iglesias, C., Soler, C., Solsona, C., Celada, A., and Felipe, A. (2003) *J. Biol. Chem.* **278,** 46307–46320; Correction (2005) *J. Biol. Chem.* **280,** 13204
9. Grissmer, S., Dethlefs, B., Wasmuth, J. J., Goldin, A. L., Gutman, G. A., Cahalan, M. D., and Chandy, K. G. (1990) *Proc. Natl. Acad. Sci. U. S. A.* **87,** 9411–9415
10. Kotecha, S. A., and Schlichter, L. C. (1999) *J. Neurosci.* **19,** 10680–10693
11. Vicente, R., Escalada, A., Soler, C., Grande, M., Celada, A., Tamkun, M. M., Solsona, C., and Felipe, A. (2005) *J. Immunol.* **174,** 4736–4744
12. Pyo, H., Chung, S., Jou, I., Gwag, B., and Joe, E. H. (1997) *Mol. Cell* **7,** 610–614
13. Jou, I., Pyo, H., Chung, S., Jung, S. Y., Gwag, B. J., and Joe, E. H. (1998) *Glia* **24,** 408–414
14. Chung, S., Lee, J., Joe, E. H., and Uhm, D. Y. (2001) *Neurosci. Lett.* **300,** 67–70
15. Khanna, R., Roy, L., Zhu, X., and Schlichter, L. C. (2001) *Am. J. Physiol. Cell Physiol.* **280,** 796–806
16. Takimoto, K., Fomina, A. F., Gealy, R., Trimmer, J. S., and Levitan, E. S. (1993) *Neuron* **11,** 359–369
17. Takimoto, K., and Levitan, E. S. (1996) *Biochemistry* **35,** 14149–14156
18. Lampert, A., Müller, M. M., Berchtold, S., Lang, K. S., Palmada, M., Dobrovinskaya, O., and Lang, F. (2003) *Pfluegers Arch. Eur. J. Physiol.* **447,** 168–174
19. Fuster, G., Vicente, R., Coma, M., Grande, M., and Felipe, A. (2002) *Methods Find. Exp. Clin. Pharmacol.* **24,** 253–259
20. Jensen, H. L., and Norrild, B. (1999) *Histochem. J.* **8,** 525–533
21. Gutman, G. E., Chandy, K. G., Grissmer, S., Lazdunski, M., Mckinnon, D., Pardo, L. A., Robertson, G. A., Rudy, B., Sanguinetti, M. C., Stühmer, W., and Wang, X. (2005) *Pharmacol. Rev.* **57,** 473–508
22. Szabo, I., Bock, J., Jekle, A., Soddemann, M., Adams, C., Lang, F., Zoratti, M., and Gulbins, E. (2005) *J. Biol. Chem.* **280,** 12790–12798
23. Snyders, D. J., Tamkun, M. M., and Bennett, P. B. (1993) *J. Gen. Physiol.* **101,** 513–543
24. Swanson, R., Marshall, J., Smith, J. S., Williams, J. B., Boyle, M. B., Folander, K., Luneau, C. J., Antanavage, J., Oliva, C., Buhrow, S. A., Bennett, C., Stein, R. B., and Kaczmarek, L. K. (1990) *Neuron* **4,** 929–939
25. Vicente, R., Coma, M., Busquets, S., Moore-Carrasco, R., Lopez-Soriano, F. J., Argiles, J. M., and Felipe, A. (2004) *FEBS Lett.* **572,** 189–194
26. Sobko, A., Peretz, A., Shirihai, O., Etkin, S., Cherepanova, V., Dagan, D., and Attali, B. (1998) *J. Neurosci.* **18,** 10398–10408
27. Shamotienko, O. G., Parcej, D. N., and Dolly, J. O. (1997) *Biochemistry* **36,** 8195–8201
28. Coleman, S. K., Newcombe, J., Pryke, J., and Dolly, J. O. (1999) *J. Neurochem.* **73,** 849–858
29. Veh, R. W., Lichtinghagen, R., Sewing, S., Wunder, F., Grumbach, I. M., and Pongs, O. (1995) *Eur. J. Neurosci.* **7,** 2189–2205
30. Klumpp, D. J., Song, E. J., Ito, S., Sheng, M. H., Jan, L. Y., and Pinto, L. H. (1995) *J. Neurosci.* **15,** 5004–5013
31. Mi, H., Deerinck, T. J., Ellisman, M. H., and Schwarz, T. L., (1995) *J. Neurosci.* **15,** 3761–3774
32. Timpe, L. C., Jan, Y. N., and Jan, L. Y. (1988) *Neuron* **1,** 659–667
33. Beeton, C., and Chandy, K. G. (2005) *Neuroscientist* **11,** 550–562
34. Freedman, B. D., Price, M. A., and Deutsch, D. J. (1992) *J. Immunol.* **149,** 3784–3794
35. Panyi, G., Bagdany, M., Bodnar, A., Vamosi, G., Szentesi, G., Jenei, A., Matyus, L., Varga, S., Waldmann, T. A., Gaspar, R., and Damjanovich, S. (2003) *Proc. Natl. Acad. Sci. U. S. A.* **100,** 2592–2597
36. Panyi, G., Vamosi, G., Bacso, Z., Bagdany, M., Bodnar, A., Varga, Z., Gaspar, R., Matyus, L., and Damjanovich, S. (2004) *Proc. Natl. Acad. Sci. U. S. A.* **101,** 1285–1290